A high-accuracy and convenient figure measurement system for large convex lens

Zhihui Tian,[*] Wang Yang, Yongxin Sui, Yusi Kang, Weiqi Liu, and Huaijiang Yang

State Key Laboratory of Applied Optics, Changchun Institute of Optics, Fine Mechanics and Physics, Chinese Academy of Sciences, Changchun, Jilin 130033, China

[*]tian-zhi-hui@163.com

Abstract: We present a novel optical configuration of a phase-shifting interferometer for high-accuracy figure metrology of large dioptric convex spherical surfaces. The conformation and design considerations according to measurement accuracy, practicability, and system errors analysis are described. More in detail, we show the design principle and methods for the crucial parts. Some are expounded upon with examples for thorough understanding. The measurement procedures and the alignment approaches are also described. Finally, a verification experiment is further presented to verify our theoretical design. This system gives full-aperture and high-precision surface testing while maintaining relatively low cost and convenient operation.

©2012 Optical Society of America

OCIS codes: (220.4830) Systems design; (120.0120) Instrumentation, measurement, and metrology; (120.6650) Surface measurements, figure; (220.1000) Aberration compensation; (120.4570) Optical design of instruments; (120.3180) Interferometry.

References and links

1. Y. Ohmura, "The optical design for microlithographic lenses," Proc. SPIE **6342**, 63421T (2007).
2. T. Matsuyama, Y. Ohmura, and D. M. Williamson, "The lithographic lens: its history and evolution," Proc. SPIE **6154**, 615403 (2006).
3. 3. http://www.qedmrf.com/metrology/products/ssi-a.
4. P. E. Murphy, G. W. Forbes, J. F. Fleig, D. Miladinovic, G. DeVries, and S. O'Donohue, "Recent advances in subaperture stitching interferometry," in *Frontiers in Optics*, OSA Technical Digest (CD) (Optical Society of America, 2006), paper OFWC2.
5. M. Bray, "Stitching interferometry–the long and winding road," in *Optical Fabrication and Testing*, OSA Technical Digest (CD) (Optical Society of America, 2010), paper OMA5.
6. P. Zhang, H. Zhao, X. Zhou, and J. Li, "Sub-aperture stitching interferometry using stereovision positioning technique," Opt. Express **18**(14), 15216–15222 (2010).
7. J. H. Burge, P. Su, and C. Zhao, "Optical metrology for very large convex aspheres," Proc. SPIE **7018**, 701818 (2008).
8. S. Chen, S. Li, Y. Dai, L. Ding, and S. Zeng, "Experimental study on subaperture testing with iterative stitching algorithm," Opt. Express **16**(7), 4760–4765 (2008).
9. Y. Dai, S. Chen, S. Li, H. Hu, and Q. Zhang, "Stylus profilometry for steep aspheric surfaces with multisegment stitching," Opt. Eng. **50**(1), 013601 (2011).
10. A. Wiegmann, M. Schulz, and C. Elster, "Absolute profile measurement of large moderately flat optical surfaces with high dynamic range," Opt. Express **16**(16), 11975–11986 (2008).
11. L. Ekstrand and S. Zhang, "Three-dimensional profilometry with nearly focused binary phase-shifting algorithms," Opt. Lett. **36**(23), 4518–4520 (2011).
12. H. Jing, L. Kuang, T. Fan, and X. Cao, "Measurement of large aspherical mirrors using coordinate measurement machine during the grinding process," Proc. SPIE **6148**, 61480I (2006).
13. V. N. Chekal', Y. I. Chudakov, and S. E. Shevtsov, "The use of coordinate-measurement machines to optimize the technology of automatic shaping of optical surfaces," J. Opt. Technol. **75**(11), 755–759 (2008).
14. J. H. Burge, "Fizeau interferometry for large convex surfaces," Proc. SPIE **2536**, 127–138 (1995).
15. B. M. Robinson and P. J. Reardon, "Distortion compensation in interferometric testing of mirrors," Appl. Opt. **48**(3), 560–565 (2009).
16. N. Bobroff, "Residual errors in laser interferometry from air turbulence and nonlinearity," Appl. Opt. **26**(13), 2676–2682 (1987).
17. C. Zhao and J. H. Burge, "Vibration-compensated interferometer for surface metrology," Appl. Opt. **40**(34), 6215–6222 (2001).

#161123 - $15.00 USD Received 10 Jan 2012; revised 30 Mar 2012; accepted 5 Apr 2012; published 25 Apr 2012

18. Z. Shi, J. Zhang, Y. Sui, J. Peng, F. Yan, and H. Yang, "Design of algorithms for phase shifting interferometry using self-convolution of the rectangle window," Opt. Express **19**(15), 14671–14681 (2011).
19. R. Jóźwicki, "Propagation of an aberrated wave with nonuniform amplitude distribution and its influence upon the interferometric measurement accuracy," Opt. Appl. **20**, 229–252 (1990).
20. S. O'Donohue, G. Devries, P. Murphy, G. Forbes, and P. Dumas, "Calibrating interferometric imaging distortion using subaperture stitching interferometry," Proc. SPIE **5869**, 156–158 (2005).
21. L. L. Deck, "Fourier-transform phase-shifting interferometry," Appl. Opt. **42**(13), 2354–2365 (2003).
22. K. Okada, H. Sakuta, T. Ose, and J. Tsujiuchi, "Separate measurements of surface shapes and refractive index inhomogeneity of an optical element using tunable-source phase shifting interferometry," Appl. Opt. **29**(22), 3280–3285 (1990).
23. G. D. Wassermann and E. Wolf, "On the theory of aplanatic aspheric systems," Proc. Phys. Soc. B **62**(1), 2–8 (1949).
24. Zygo is a registered trademark of Zygo Corporation.

1. Introduction

Modern optical lithography techniques require large ultra-precision lenses. The ability to produce them to more exacting operational specifications is demanded by designers [1,2]. For example, micro-lithographic lenses for the ArF optics generation often have large diameter (200–300 mm) dioptric components. It is common now that manufacturers receive requests for optics with a surface roughness of several angstrom rms and overall figure accuracy of better than 1 nm. Among them, figure measurements of large convex surfaces are notoriously undesirable because it requires that the clear aperture (CA) and the numerical aperture (NA) of transmission spheres (TS) must be larger than the CA and the NA of the surfaces to be tested. On the other hand convex surface testing is frequently encountered, because the number of convex surfaces is often greater than the concave surface number in optical systems as the total optical power is usually greater. There are many problems in the design and fabrication of those TS lenses. They are often very bulky, heavy, and expensive. Furthermore, there are some TS (with very large NA and CA) that could not be manufactured nowadays. To demonstrate the above situation, we show a 12 inch, 218 mm radius 0.82F-number TS lens in Fig. 1 that we have designed.

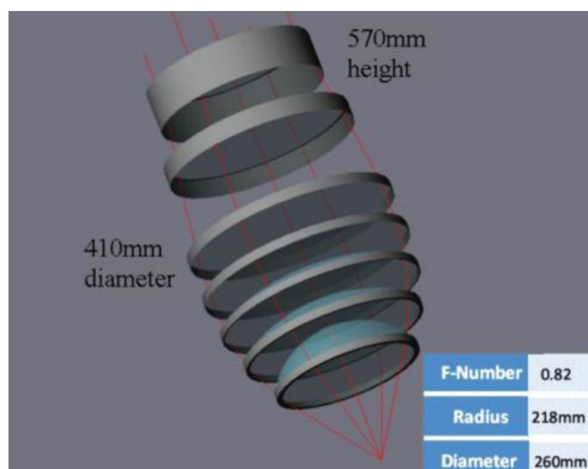

Fig. 1. Data of our 12 inch F/0.82 transmission sphere lens.

There are some other methods that can also be used to test large convex surfaces, such as sub-aperture stitched interferometric metrology [3–8], profile measurement [9–11], and use of a coordinate measurement machine [12,13], for example. But those methods can hardly realize high precision (nm level) and a large measuring range (very large NA and CA) at the same time. J. H. Burge roughly described a measurement method for a 270 mm convex sphere with 0.6 NA by using an f/0.6 TS, a lens that had one surface concentric with the test plate and a reflection surface for reference [14]. This method could be implemented at low cost, but

#161123 - $15.00 USD Received 10 Jan 2012; revised 30 Mar 2012; accepted 5 Apr 2012; published 25 Apr 2012
(C) 2012 OSA

there were four nearly concentric surfaces. To avoid multi-beam interference, the Fizeau reference and the imager surface were tilted in order to have the reflections from those surfaces be blocked. Tilting would destroy the transmission wavefront. After tilting, the wavefront errors, wavefront slope errors, reverse-direction imaging distortion, and instrument transfer function (ITF) were not the same as those before. It is hard to know the variations of those factors because there was no interference until a reference surface was installed. In high-accuracy measurements, those factors are very important for calibrations and compensations for systematic errors. In addition, the structure is inconvenient for tilt adjustment because of the lack of a closed loop. All of these affected the measurement accuracy.

In this paper we propose a new alternative measurement system for large dioptric convex spherical surfaces in high-accuracy tests. In optics, there are two main parts–the main test bed and the attachment for lens testing. The main test bed includes an ordinary Fizeau illumination, a wavelength-stepping phase-shifting technology, an "optical flat in or out" architecture, and a diverger lens with a special design that is different than an ordinary TS. The flat plate can move into or out from the light path according to need. The attachments for our measurement system are a series of concise optical systems that compensate for the spherical aberration of the test lens. Here we call them a spherical aberration compensation system (SACS). The SACS is similar to a null corrector in an aspheric surface null test, but it has a few differences in design principles and methods. The tolerances are also not so rigorous. The "optical flat in or out" architecture can avoid multi-beam interference without lowering measurement accuracy. So, our measurement system can utilize both time and frequency domain phase-shifting algorithms. This approach can have a significantly greater flexibility and higher measurement precision than previous methods as well as give relatively low cost and convenient operation. It can easily test convex surfaces that work downward without analyzing the gravity. The paper is organized as follows. Section 2 shows the basic theory principle, system configuration, and error analysis of our metrology system. In Section 3 we describe the optical alignment approach and the measurement procedure, while details of the optical design followed by several representational cases for the test bed and its matched SACS are given. In Section 4 the presentation of a demonstration measurement and the experimental results are offered for verifying our design. Finally, a brief summary and conclusions are given in Section 5.

2. Description of the system configuration and the theory principle

The figure measurement system utilizes Fizeau coherent illumination and wavelength-stepping phase-shifting technology. By using a tunable laser, the phase shifting can be faster and more stable. A schematic diagram of the main test bed is depicted in Fig. 2. Here, we construct an ordinary 50 mm diameter CA Fizeau interferometry, an optical flat plate that has an exceptional optical-quality surface, $\lambda/40$ peak to valley (PV) or better, with no AR coating and an f/0.8 diverger lens that is distinguished from an ordinary TS because it has no reference surface. The main part of the test bed has small dimensions, so it is easy to achieve good optical quality while keeping the cost low. Following the main test platform, there is an auxiliary measure optical system (SACS) that can compensate for the spherical aberration introduced by the lens to be tested (not drawn in Fig. 2 but will be seen later on). The component to be tested is optically arranged after SACS, and together they constitute a big generalized TS lens. A concave reference sphere is then located close to the test surface and they constitute a short test cavity together. Because systematic errors are mostly limited by the ability to figure and measure the concave reference sphere, it must be of good quality and measured to high accuracy. When the optical flat is "in" and the reflection reference is "out", the two interferometric surfaces are the flat surface and the test surface. The objective of this stage is testing and finely adjusting the transmission wavefront errors, wavefront slope, reverse-direction imaging distortion, and ITF of "the general large TS", which is composed of the diverger lens, the SACS, and the test plate. For high-accuracy testing, this is important to

#161123 - $15.00 USD Received 10 Jan 2012; revised 30 Mar 2012; accepted 5 Apr 2012; published 25 Apr 2012
(C) 2012 OSA

calibrate for retrace errors and systematic errors. When the optical flat is "out" and the reflection reference is "in", the two interferometric surfaces are the reflection reference surface and the test surface. The objective of this is testing the figure. The small hole located at the focus of the diverger lens can cut off most of the stray light, which is advantageous to improve test precision. If there is any residual aberration in the imaging module, it will cause distortion and influence measurement [15], so we must control it in the design stage. As we know vibration, airflow, and temperature deter us in reducing the uncertainty [16,17]. Here, using a short interference cavity is very helpful in order to suppress them.

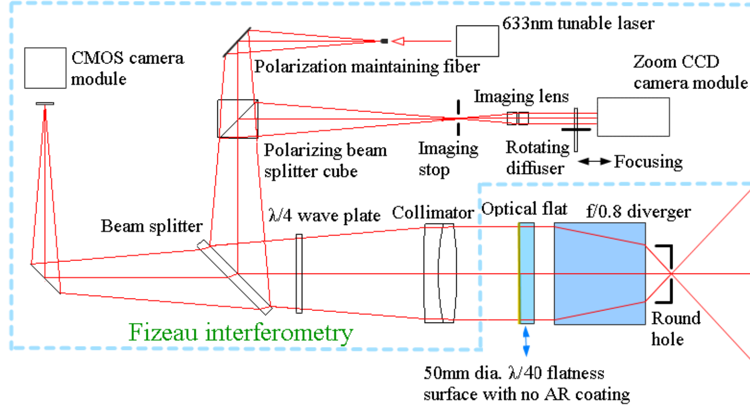

Fig. 2. Mainframe of our new type of test bed for large convex surface.

Here we use a 633 nm tunable laser as the illumination source. The fringe pattern obtained from the CCD camera for a single test surface can be expressed as

$$g(x,y)=a_0(x,y)+a_1(x,y)\cos[\frac{2\pi}{\lambda}L(x,y)],\tag{1}$$

where $g(x, y)$ is the intensity at a pixel positioned at point (x, y), $a_0(x, y)$ is the background, $a_1(x, y)$ is the modulation, and L is the optical path difference of the testing surface and the reference mirror. If a tunable laser is used by the interferometer to change the wavelength from λ to λ-$\Delta\lambda_m$, the intensity of the interferogram becomes

$$g_m(x,y)=a_0(x,y)+a_1(x,y)\cos[\frac{2\pi}{\lambda-\Delta\lambda_m}L(x,y)].\tag{2}$$

This can be rewritten as

$$g_m(x,y)=a_0(x,y)+a_1(x,y)\cos[\frac{2\pi}{\lambda}L(x,y)+\frac{2\pi\Delta\lambda_m}{\lambda(\lambda-\Delta\lambda_m)}L(x,y)],\tag{3}$$

where g_m is the mth acquisition of the interferogram and $\theta_m=\frac{2\pi L(x,y)\Delta\lambda_m}{\lambda(\lambda-\Delta\lambda_m)}$ is the mth phase shift. For short interferometric cavity measurement, we assume $L=10$ mm and standard 13 steps phase shifting $\lambda-\lambda_m\approx\lambda=633$ nm, $m=13$, and $\theta_m=13\times{}^{\pi}\!/_{4}={}^{13}\!/_{4}\pi$. We get that in one phase-shifting period, the shifting wavelength bandwidth is $\Delta\lambda_m\approx0.07$ nm, and the bandwidth will be much narrower in the long cavity measurement. For a high-precision test, it is better to correct the chromatic aberration in the system, and it is not too hard to correct chromatic aberration for so narrow a bandwidth. The imperfect performance of hardware, phase-shift errors caused by laser's nonlinearity, and high-order harmonics caused by the

#161123 - $15.00 USD Received 10 Jan 2012; revised 30 Mar 2012; accepted 5 Apr 2012; published 25 Apr 2012
(C) 2012 OSA

CCD's nonlinearity usually introduce errors in retrieving information from the test plate. To solve this problem, the laser and CCD must be calibrated, and we plan to use a new phase-shifting algorithm [18] that is error-resistant to these error sources. Furthermore, the algorithm can also suppress the effects of error sources from metrology environments including vibration, airflow, and temperature instability.

3. Details of optical design and measurement procedure

3.1 Diverger lens design

The diverger lens in this system has two major roles. One function is that it first has to converge on the nearly parallel coming beam at its focus point, and then it diverges light. By doing so, it transforms the plane wavefront into an ideal spherical wavefront. This diverger can be small in dimension and can be distinguished from ordinary TS because all of its surfaces have been coated with a high-AR coat. It does not have a reference surface, which is exceptional in optical quality, and has to keep concentric with the transmission wavefront. So, it is superior in price, aberration correction, fabrication, and testing precision. For the diverger lens design, the major aberrations that need to be corrected are spherical aberration, coma, and some chromatic aberration because of wavelength-shifting bandwidth.

According to aberration theory, spherical aberration and coma highly rely on CA, and a smaller aperture (50 mm) can reduce advanced aberrations and wavefront slope errors. The surface refraction law of the lens in air is expressed as

$$\sin\theta = n\sin\theta', \tag{4}$$

$$\Delta\theta = \theta' - \theta. \tag{5}$$

For the f/0.8 diverger, we assume that there are i surfaces, so the total deflection angle is invariable.

$$\Delta\theta_{total} = \arctan\left(\frac{1}{2\times 0.8}\right) - 0 = 32° = \sum_{1}^{i}(\theta_i' - \theta_i). \tag{6}$$

From this we can see that a high refraction index is favorable for lower θ and θ' and thus reduces aberrations as the nonlinearity. Here we use 3 pieces of a ZF6 lens with a relatively high refraction index and a piece of K9 lens to correct monochromatic aberration and chromatic aberration (Chinese glass). The optimization merit function is written as "MeritFunction1".

The other function of a diverger lens is interference imaging. Here, the light path direction is opposite to the illumination module. As part of an imaging system, a diverger with other elements, such as a collimator and the imaging lens, together project the test surface onto the detector. An aberrated wavefront continuously changes its shape as it travels. Thus, if the optical system is not perfect, the interference pattern will also continuously change as the beam propagates [19]. Hence, the interferogram should be taken at the place of the test surface. Since only a narrow pencil of rays actually scatter from each point of the test surface and the residual aberrations are very small in the diverger, they will not blur the interferogram severely, while the diverger may cause distortion in imaging without careful considerations. The distortion is influential for two reasons. Surface measurements are usually made to guide the fabrication. It is important that the optician knows where the surface irregularities really are so he can effectively polish them out. Imaging distortion also causes low-order alignment errors (tilt, focus) to appear as higher-order surface errors [15,20]. Presume that ρ_c is the radial position in the image coordinate, ρ_t is radial position in the object coordinate, m is the magnification from object to image, and ε is the distortion coefficient. As a result, the radial displacement caused by distortion is expressed as

$$\Delta\rho_c = \rho_c' - \rho_c = m\varepsilon\rho_t^3. \tag{7}$$

#161123 - $15.00 USD Received 10 Jan 2012; revised 30 Mar 2012; accepted 5 Apr 2012; published 25 Apr 2012
(C) 2012 OSA

Distortion influences measurement accuracy by changing the wavefront, which is measured using a series of orthogonal polynomials to express the measured wavefront as

$$W(\rho,\theta)=\sum_{n,k} a_{nk}\rho^{n}\cos k\theta+b_{nk}\rho^{n}\sin k\theta. \tag{8}$$

Since ε is usually very small in a deformed wavefront, let $(1+\varepsilon)^{n}\approx 1+n\varepsilon$, and then we get the following relation:

$$a_{n}\rho'^{n}\rightarrow a_{n}\rho^{n}+a_{n}n\varepsilon\rho^{n+2}. \tag{9}$$

Thus, it can be seen that lower-order aberrations will generate higher aberrations because of imaging distortion, and the higher aberrations are proportional to distortion coefficient ε.

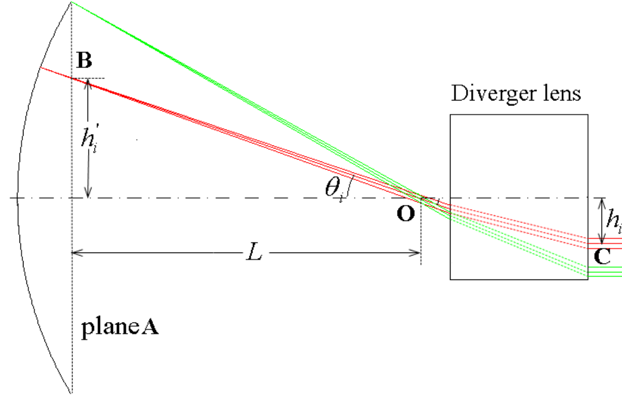

Fig. 3. Curved object imaged through diverger.

The light propagation directions of the above two are opposite. It would be best to control the reverse-direction distortion and optimize the transmission wavefront at the same time in the design stage. But, in commercial optical design software, conventional multi-configuration (zoom) optimization can hardly solve this problem. Here, we show an efficacious approach using a single optimization configuration. Figure 3 simply illustrates a curved object imaged through a diverger lens. The principal ray of a fine pencil imaging beam from each position of an object hits the optical axis at point *O*, which is the site of the stop. Plane *A* plumbs the optical axis and passes through both ends of the object. The distance between plane *A* and point *O* is *L*. The imaging system focus is on plane *A*, the intersection of principal rays from object points with plane *A* is *B*, and the intersection of principal rays with the outermost surface of the diverger is *C*. Assuming the focal length of the diverger is *f*, the magnification is *m*, the angle between principal rays and optical axis is θ, the distance from *B* to optical axis is *h'*, and the distance from *C* to optical axis is *h,* we get that

$$m=\frac{h'}{h}=\frac{L}{f}. \tag{10}$$

For different field points, if imaging distortion is nonexistent, these are the following relationships:

$$h_i'=L\cos\theta_i, \tag{11}$$

$$h_i=f\cos\theta_i, \tag{12}$$

$$\cos\theta_i=\frac{h_i}{f}. \tag{13}$$

According to the above analysis, we construct the merit function for optimizing to minimize imaging distortion:

$$\text{Merit function} = \sum_{1}^{i} \left| \cos\theta_i - \frac{h_i}{f} \right|. \tag{14}$$

The optimization merit function is written as "MeritFunction2".

Finally, we use the optimized results of MeritFunction1 to be the initial structure, and we optimize the diverger lens again by using a new error function, which is

$$\text{Merit function} = w_1 \cdot Meritfunction1 + w2 \cdot Meritfunction2. \tag{15}$$

w_1 and w_2 are weighting factors. w_2 can be much larger than w_1 for different units.

The results are presented in Fig. 4 and Table 1.

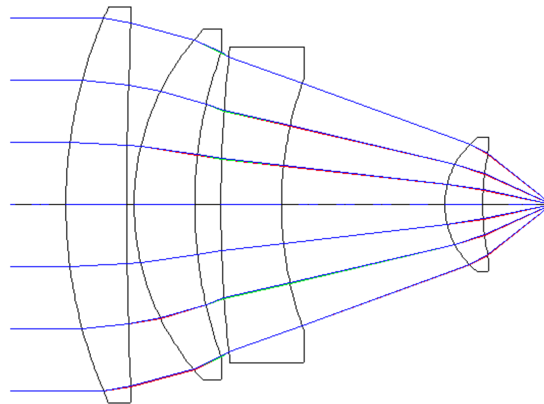

Fig. 4. Layout of optical design results for f/0.8 diverger lens in our measurement system.

Table 1. Lens System Prescription for f/0.8 Diverger

Surface	Radius (mm)	Thickness (mm)	Glass	Clear Aperture (mm)
1	65.210	8.00	ZF6	50.00
2	494.300	1.00		48.80
3	34.850	8.00	ZF6	44.30
4	61.170	3.45		41.00
5	187.630	8.00	ZF6	39.65
6	49.430	21.55		32.60
7	11.512	5.00	K9	16.30
8	35.520			13.65

3.2 Measurement procedure

The testing figure**[Au: Do you mean 'process' instead of 'figure' here? Please clarify.]** of a large dioptric convex spherical surface with our measurement system is composed of two main steps. In Step 1, the SACS and the lens to be tested are installed and adjusted through monitoring interferograms, which are produced by the back bare surface of the optical flat and the test surface. Computer auxiliary adjustment methods and other similar skills can be used to control the relative positions. The main judgment standard is wavefront slope error. Because this part is not in the cavity in the final measurement stage (Step 2) and can be calibrated, this is not too rigorous. Other judgment standards like distortion are also helpful. In Step 2, the optical flat is moved out of the light path; then, we install and adjust the reference

#161123 - $15.00 USD Received 10 Jan 2012; revised 30 Mar 2012; accepted 5 Apr 2012; published 25 Apr 2012
(C) 2012 OSA

sphere and measure the figure of the test surface by wavelength phase shifting. Figure 5 illustrates that process. The reference surface and the back bare surface of the optical flat must be carefully calibrated before testing, as systematic errors are mostly limited by the ability to figure and measure the concave reference surface. Systematic optical path difference (OPD) error is a combination of an imperfect illumination wavefront, reference surface figure error, imaging aberrations depending on field and pupil, the ITF, and so on. Thus for high-accuracy measurements, system error calibrations are necessary. And, a long thermalization time is a prerequisite to reach nanometer range uncertainty.

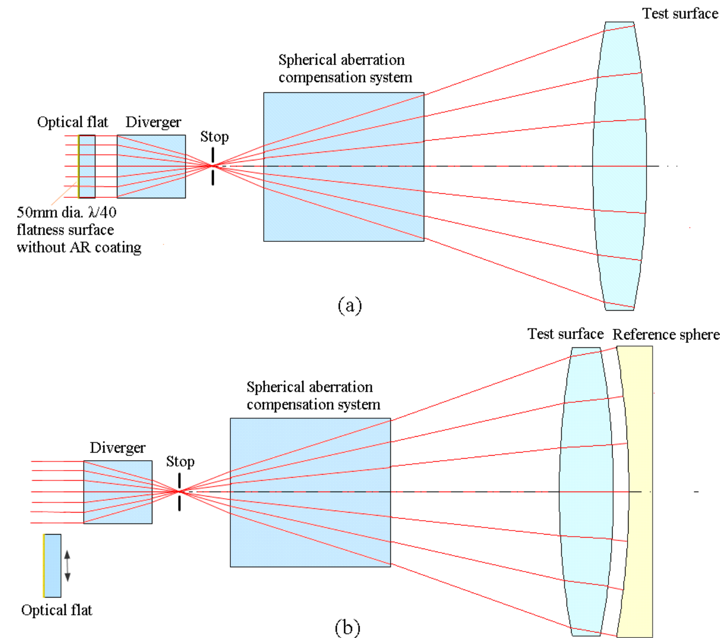

Fig. 5. Test setup to measure the figure of a large dioptric convex spherical surface with our measurement system. The testing process is composed of two main steps. (a) Step 1: SACA and the lens to be tested are installed and adjusted through monitoring interferograms, which are produced by the back bare surface of the optical flat and the test surface. (b) Step 2: move the optical flat out of light path, install and adjust the reference sphere, and measure figure of test surface by wavelength phase shifting.

The measurement procedure is summarized below:

1. Primary arrangement of the SACS and the test lens. The stop hole integrated in diverger lens is used as a coarse coordinate to locate the SACS and the test lens, and then the two elements are adjusted while we observe location changes of the light points in auxiliary adjustment module through a CMOS camera until we get a good result.

2. Fine adjustment of the diverger lens, the SACS and the test lens. Here, the two interference surfaces are the back bare surface of the optical flat and the test surface; therefore, we can use interferograms produced by those two surfaces to guide the adjustment. The imaging module is focused on the pupil of the optical system, and a phase-measuring algorithm is used to get quantities of the wavefront. Computer auxiliary adjustment methods may be used for multi-component cases. The object of this section is to generate a fairly perfect wavefront transmitted through and reflected at the test surface, and thus the wavefront slope errors may be the objective function. The weak reflection of the optical flat plate can be ignored for wavefront slope

#161123 - $15.00 USD Received 10 Jan 2012; revised 30 Mar 2012; accepted 5 Apr 2012; published 25 Apr 2012
(C) 2012 OSA

measurement, and the front surface may be slightly tilted but smaller than the wedge angle of ordinary TF for further improvement.

3. Move the optical flat out of light path, then install and adjust the reference sphere. In this section, the two interference surfaces are the test surface and the reference sphere surface, while the imaging module is focused on the test surface. The adjustment means can be similar to those in Section 2.

4. Measuring figure of the test surface by wavelength phase shifting. Here, the wavelength phase-shifting method and algorithm we used is by wavelength stepping and suffers from fundamental limitations in two-beam interference. There are some other wavelength phase-shifting styles and algorithms based on frequency domain that can also be used in handling multiple-surface interference [21,22]. So, the measurement results can be compared. But the cavity lengths are restricted by specific expressions, and thus they are a little inconvenient in practice.

3.3 Spherical aberration compensation system (SACS)

The SACS is one of crucial parts in the test system. Its major effect is compensating for the spherical aberration generated from the other surface, which is not being tested with the test dioptric lens. So the transmission wavefront can be perpendicular to the test surface as well as matched with the diverger.

Figure 6 draws a case of single surface refraction, where each parameter is indicated. According to aberration theory, spherical aberration of single-refraction surface is expressed as

$$\delta L' = \frac{n_1 u_1 \sin U_1}{n_k' u_k' \sin U_k'} \delta L_0 - \frac{1}{2 n_k' u_k' \sin U_k'} \sum_1^k S_- = -\frac{1}{2 n_k' u_k' \sin U_k'} \sum_1^k S_-, \tag{16}$$

$$S_- = \frac{niL \sin U (\sin I - \sin I')(\sin I' - \sin U)}{\cos \frac{1}{2}(I - U) \cos \frac{1}{2}(I' + U) \cos \frac{1}{2}(I + I')}. \tag{17}$$

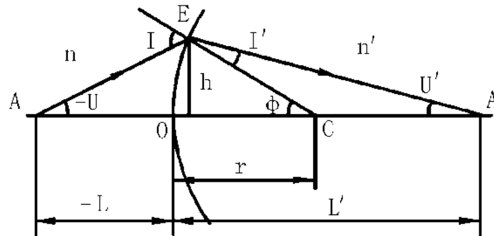

Fig. 6. Sketch map of single-surface refraction.

For the test lens, when the test light beam is reflected and propagates backward to the interferometer, if the test surface is perfect, rays are perpendicular to it. The incidence angles are $I = 0$. Thus it doesn't introduce any spherical aberration. So, the total spherical aberration of the test lens equals the spherical aberration introduced by the other surface. According to Eq. (16) and Eq. (17), we can simply estimate the spherical aberration quantity introduced by the lens to be tested in our measurement system by comparing the curvature difference of its two surfaces. To illustrate this, we show spherical aberrations introduced by four types of test lenses whose forms are concentric, meniscus, plano-convex, and bi-convex in Fig. 7. The spherical aberrations are progressively increased.

#161123 - $15.00 USD Received 10 Jan 2012; revised 30 Mar 2012; accepted 5 Apr 2012; published 25 Apr 2012
(C) 2012 OSA

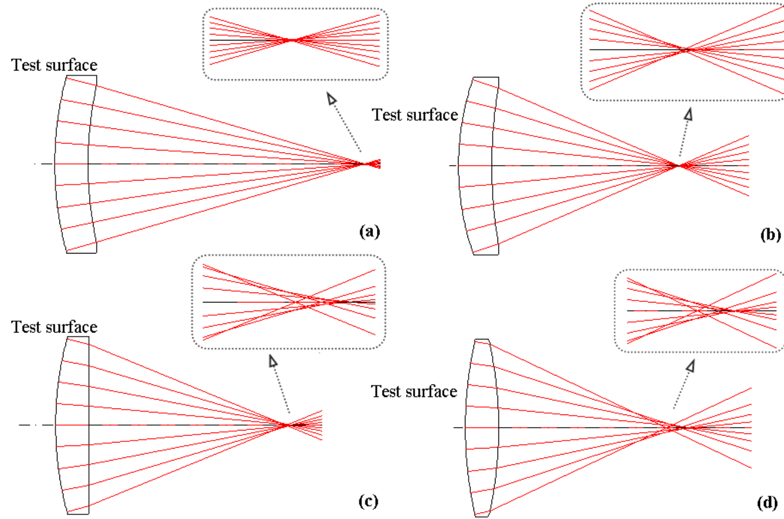

Fig. 7. Spherical aberrations introduced in four types of test lenses; the test surface is perpendicular to the rays, so it has no spherical aberrations. (a) Concentric lens, (b) meniscus lens, (c)plano-convex lens, (d) bi-convex lens.

In Eq. (17), when the spherical aberration is $\delta L'=0$, it can create three cases, called aplanatism.

$$\begin{aligned}&(1) L=0, L'=0,\\&(2) \sin I-\sin I'=0, I=I'=0,\\&(3) \sin I'-\sin U=0, I'=U, L=(n+n')r/n, L'=(n+n')r/n'.\end{aligned} \tag{18}$$

Thus, SACS can merely be a simple lens that has the same optical material with the lens to be tested. One surface of the compensation lens is very close to the test lens, and the other surface conforms to one of the three conditions in Eq. (18). The test lens and the compensation lens together compose an aplanatic lens. Figure 8 shows a lens having a convex surface to be tested and the three types of aplanatic spherical aberration compensation lenses. For the first case, it wastes too much material. The focus is on the back surface. Thus, there is a cat-eye condition, which should be avoided. So, the first case is improper. Similarly, the second case is not very proper because it contains a confocal condition. Therefore, we recommend the third type of compensation lens as it does not contain a confocal or cat-eye condition. Another benefit of the third type of compensation lens is that it can also expand the NA. The magnification can be calculated as

$$\beta=\frac{NA'}{NA}=n, \tag{19}$$

where n is the index of refraction. So, we can test a large NA surface with a smaller NA diverger. For example, an NA = 0.9 convex surface can be test by a diverger lens.

$$NA=\frac{0.9}{1.5}=0.6. \tag{20}$$

#161123 - $15.00 USD Received 10 Jan 2012; revised 30 Mar 2012; accepted 5 Apr 2012; published 25 Apr 2012
(C) 2012 OSA

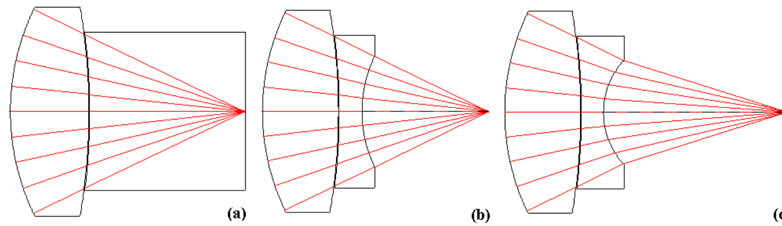

Fig. 8. Lens having a convex surface to be tested and its three types of aplanatic spherical aberration compensation lenses; (a) $L = 0$, (b) $I = I' = 0$, (c)$L = (n + n')r/n$, $L' = (n + n')r/n'$.

As an example, we design a spherical aberration compensation lens to test a 260 mm convex sphere with f/1.0; the design results are presented in Fig. 9 and Table 2. What needs to be mentioned here is that although the two lenses are very close, there is still a small air gap between them, and it introduces spherical aberration. Usually, this value is very small, and we do not have to care about it. But when the angle of the marginal ray at the air gap is large, the spherical aberration also becomes large. In this situation, liquid can be used to fill the gap. Although the optical material of the spherical aberration compensation lens is the same as the test lens, the quality of the material can be lower, for the compensation lens is outside the interferometric cavity in the figure measurement stage.

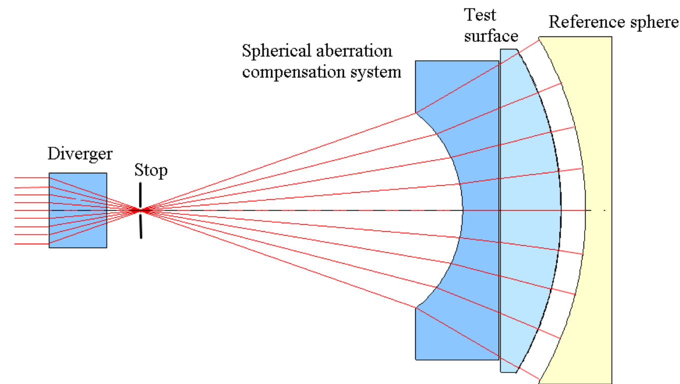

Fig. 9. Spherical aberration compensation lens design for a 260 mm f/1.0 convex spherical surface.

Table 2. Data of 260 mm f/1.0 Convex Surface and Its Spherical Aberration Compensation Lens

Surface	Radius (mm)	Thickness (mm)	Glass	Clear Aperture (mm)
1	−103.00	30.00	Fused quartz	180.00
2	Infinity	1.00		245.00
3	Infinity	50.00	Fused quartz	245.00
4	−260.00	20.00		260.00
5	−280.00			280.00

An aplanatic spherical aberration compensation lens is easy to design and can compensate for spherical aberrations of nearly all types of large convex lenses. But this type of spherical aberration compensation lens is usually somewhat large and weighty. Thus there is some

#161123 - $15.00 USD Received 10 Jan 2012; revised 30 Mar 2012; accepted 5 Apr 2012; published 25 Apr 2012
(C) 2012 OSA

inconvenience in making adjustments. SACS can also be composed of several small lenses. They are more controllable and optical material selection is more flexible, so they can correct chromatic aberration, spherical aberration, and coma more thoroughly and sometimes can be more inexpensive. They are similar to null lenses used in aspheric surface metrology, while the tolerances are looser than null lenses as they locate in the common light path part.

We suppose there are k pieces of the lens in the spherical aberration compensation lens, and we can obtain the spherical aberration for different aperture height y:

$$SphT = \sum_{1}^{k} \frac{(n-1)l_2^{'}}{2n^2 y_2}[(\frac{1}{r_1} - \frac{n+1}{l_1})(\frac{1}{r_1} - \frac{1}{l_1})^2 y_1^4 - (\frac{1}{r_2} - \frac{n+1}{l_2^{'}})(\frac{1}{r_2} - \frac{1}{l_2^{'}}) y_2^4]. \quad (21)$$

The subscripts 1 and 2 represent front and back surfaces of a lens. For aperture spherical aberration compensation,

$$SphT_{test} + SphT_{compensation} = SphT_{test} + SphT = 0. \quad (22)$$

We design a simple spherical aberration compensation lens of this type to test a 260 mm convex sphere with 500 mm curvature radius, for instance. The lens design results are presented in Fig. 10 and Table 3.

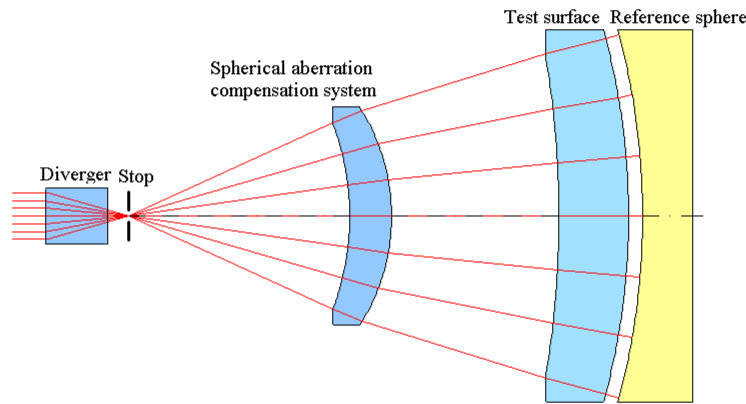

Fig. 10. SACS design for a 260 mm 500 mm curvature radius convex spherical surface.

Table 3. Lens System Prescription for Designing a SACs of a 260 mm 500 mm Curvature Radius Convex Spherical Surface

Surface	Radius (mm)	Thickness (mm)	Glass	Clear Aperture (mm)
1	−187.180	30.00	ZF2	136.00
2	−143.913	120.00		153.00
3	700.000	50.00	Fused quartz	237.00
4	500.000	10.00		260.00
5	510.000			270.00

Since the tolerances of the compensation system are not so harsh, we may barely use a small piece of the aspheric lens with good quality of surface-middle frequency as a simple SACS. Methods, such as used in reference [23], may be helpful. Here, we do not plan to describe this in detail due to the length of paper. Besides aspheric lenses, some new types of

#161123 - $15.00 USD Received 10 Jan 2012; revised 30 Mar 2012; accepted 5 Apr 2012; published 25 Apr 2012
(C) 2012 OSA

optical devices may be used, such as zone plates, hybrid refractive-diffractive lenses, and a computer-generated hologram (CGH). Moreover, dynamic programmable optical devices may also be used; for instance, a liquid-crystal display (LCD) as a phase modulator, a liquid tunable lens, even MEMS-based optical components, because they are very flexible and operational. Here we present a CGH-type SACS that matches with a bi-convex lens, where the test surface is a large convex lens with 260 mm CA and 500 mm curvature radius. The optical system prescriptions are shown in Fig. 11 and Table 4. Most other no-measurement diffraction-order light of the CGH can be blocked by a stop.

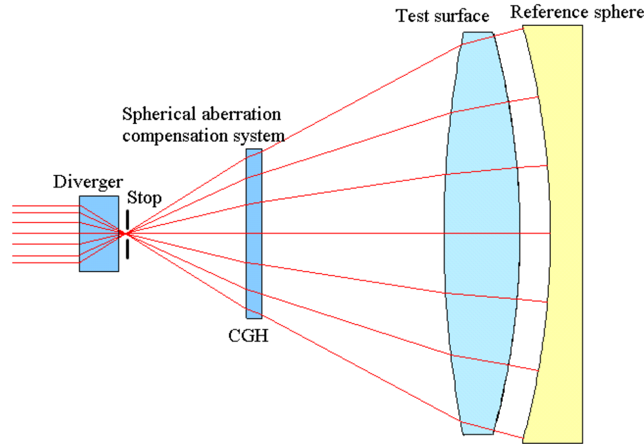

Fig. 11. CGH-type SACs design for a 260 mm 500 mm curvature radius convex spherical surface of a bi-convex lens.

Table 4. Data of a CGH Type SACs for a 260 mm 500 mm Curvature Radius Convex Spherical Surface of a Bi-convex Lens

Surface	Radius (mm)	Thickness (mm)	Glass	Clear Aperture (mm)
1	Infinity	10.00	Fused quartz	100.00
2	Infinity	120.00		108.00
3	–700.00	50.00	Fused quartz	250.00
4	500.00	20.00		260.00
5	520.00			270.00

4. Verification experiment

4.1 Experimental setup

For verifying parts of our design, we set up a simple experimental system. The test surface is comparatively small but symbolical. The experimental setup is shown in Fig. 12 and Fig. 13 below. It consists of a 4-inch Zygo MST interferometer [24], a TS lens, a SACS; the lens is enclosed by the test surface and a reference surface of another TS. Here there are three interference surfaces–the TS surface (S1), the test surface (S2), and the RS (S3). Thus, there are a total of three interference cavities: S1S2, S1S3, and S2S3. The MST interferometer can handle multi-surface interferometric cavities by using a Fourier-based analysis technique combined with wavelength tuning. The cavity lengths are restricted by specific expressions, as mentioned above. By specially designing the parameters of the spherical aberration compensation lens and changing the length of the testing cavity S2S3, we can get $L_1 = 3L_2$, where L_1 is the cavity length of S1S2 and L_2 is the cavity length of S2S3. Then we select the "$L_1=3L_2$" option in the test software menu and do the measurement. We integrate the SACS

#161123 - $15.00 USD Received 10 Jan 2012; revised 30 Mar 2012; accepted 5 Apr 2012; published 25 Apr 2012
(C) 2012 OSA

and the test surface, which can be seen in Fig. 14. The measurement results are compared with the results of traditional large-TS test procedures. The traditional system is shown in Fig. 14. It consists of a 4-inch Zygo MST interferometer, the same transmission sphere used in our experiment system, and the test plate. The measurement results from the both systems are compared. Because we use the same reference surface, we did not calibrate the reference surface, so it is simple to compare the results of the test surface.

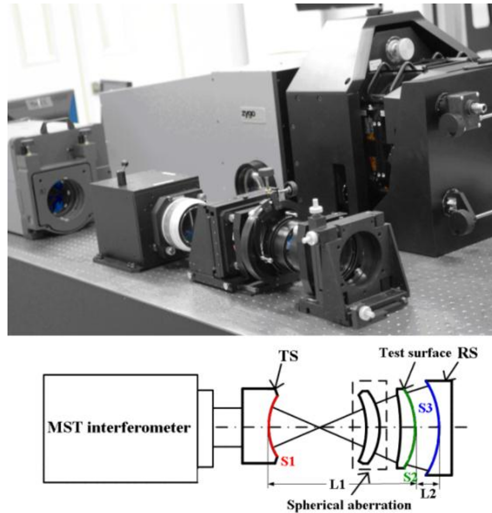

Fig. 12. Photograph of new system's experimental setup.

Fig. 13. Photograph of integration of the SACS and the lens enclosed by the test surface.

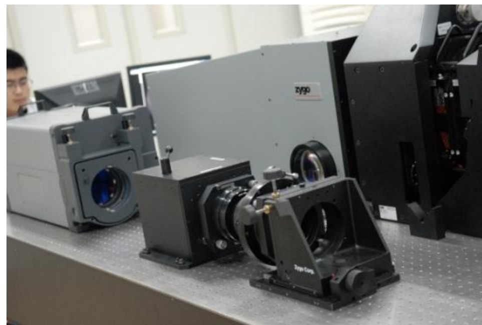

Fig. 14. Photograph of traditional system.

4.2 Experimental results

The experimental results of the new system are illustrated in Fig. 15(a). We acquire 10 consecutive measurements with the new system and average the 10 with a 95% auto aperture. The mean rms of those measurements is 6.15 nm. The repeatability of the rms is 0.46 nm (2σ). In a similar way, we also acquire 10 consecutive measurements with a traditional system. The results are shown in Fig. 15(b). The mean rms of those measurements is 5.74 nm. The repeatability of the rms is 0.62 nm (2σ). The difference in the rms repeatability of both systems is small. It indicates that the stability of both systems is not obviously different. We subtract the mean figure map from the other and acquire the result shown in Fig. 15(c). The rms of the result is 1.19 nm. It denotes that the systematic error of the new system should be small. But it is a relatively large error for micro-lithographic lens metrology. We think if the surrounding stability (vibration, temperature, etc.) and the mounting repeatability are better, then the results acquired are more persuasive. After comparing both systems, we conclude that the new system is feasible and usable.

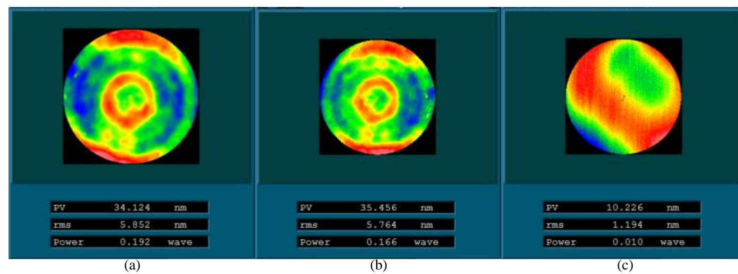

Fig. 15. Experiment results. (a) The result from the new system. (b) The result from the traditional system. (c) The difference of the figure maps measured by both systems.

5. Conclusion and discussion

In summary, we have presented a new optical figure measurement system for large dioptric convex surfaces. The theory analysis, the optical alignment, the test procedures, and the design details have been described, and some typical application cases have been given. Since there are relatively fewer error sources and the elements used for metrology are operational, the system can realize high precision and low cost. This design has been experimentally shown to be of good validity. In addition, what should be pointed out here is that our current work is concentrated on convex spherical surfaces, but this approach may also extend its application field to testing convex aspheric surfaces by using a concave aspheric reference, which is easier to measure. Future work will concentrate on the realization of programmable SACS and how to integrate them to the main test bed.

Acknowledgments

The authors thank the National Hi-tech Research and Development Program of China (2009ZX02205-004) for their financial support. We heartily thank Mr. Chunlai Liu for his aid to us in performing the experiment.

#161123 - $15.00 USD Received 10 Jan 2012; revised 30 Mar 2012; accepted 5 Apr 2012; published 25 Apr 2012
(C) 2012 OSA